THE EUV CHROMOSPHERIC NETWORK IN THE QUIET SUN

E. M. REEVES

Center for Astrophysics
Harvard College Observatory and
Smithsonian Astrophysical Observatory
Cambridge, Mass. 02138, *U.S.A.*

(Received 12 October, 1975)

Abstract. Investigations on the structure and intensity of the chromospheric network from quiet solar regions have been carried out with EUV data obtained from the Harvard spectroheliometer on the Apollo Telescope Mount of Skylab. The distribution of intensities within supergranulation cell interiors follows a near normal function, where the standard deviation exceeds the value expected from the counting rate, which indicates fine-scale structure below the 5 arc sec resolution of the data. The intensities from the centers of supergranulation cells appear to be the same in both quiet regions and coronal holes, although the network is significantly different in the two types of regions. The average halfwidth of the network elements was measured as 10 arc sec, and was independent of the temperature of formation of the observing line for $3.8 < \log T_e < 5.8$. The contrast between the network and the centers of cells is greatest for lines with $\log T_e \approx 5.2$, where the network contributes approximately 75% of the intensity of quiet solar regions. The contrast and fractional intensity contributions decrease to higher and lower temperatures characteristic of the corona and chromosphere.

1. Introduction

Solar observations of the visible disc of the Sun from ground-based instrumentation, when narrow band filters are used to select specific wavelength emissions (such as Hα or Ca II), reveal a wealth of structural detail arising primarily from the layers of the photosphere and low chromosphere. The size of the observed structure ranges down to the limits of the instrumental resolution or seeing conditions, with Hα structure such as spicules observed at a resolution of several tenths of a second of arc, corresponding to dimensions of several hundred kilometers. Observations of the Sun from above the Earth's atmosphere permit the study of solar phenomena over a much greater range of temperature, extending through the chromosphere, transition region, and into the corona, but the resolution is limited by both technology and signal levels. The solar instrumentation in the Apollo Telescope Mount (ATM) on Skylab provided extensive observations over nearly 9 months and extended from the visible region, through the ultraviolet, and into the X-ray region (Reeves *et al.*, 1972), with a spatial resolution of several arc seconds, the best resolution yet achieved in the non-visible region.

The observations of quiet areas on the solar disc described here were carried out with the Harvard College Observatory spectrometer on the ATM. The instrument covered the wavelength range 250–1350 Å with a spatial resolution of

Solar Physics **46** (1976), 53–72. *All Rights Reserved*
Copyright © 1976 by D. Reidel Publishing Company, Dordrecht-Holland

5 arc sec, and was optimized to observe the characteristic radiations from the chromosphere, transition region, and lower corona; that is, to observe the emission spectrum of lines and continua formed over the temperature range from 10^4 to 3×10^6 K. The instrument was provided with dual capabilities to obtain spectral scans of the full wavelength range with a spectral resolution of 1.6 Å (full width at half maximum intensity for a narrow line) in under 4 min, or alternatively, to obtain data in a spectroheliogram mode within a 5 arc min square field in 5.5 min with the same spatial resolution. In the spectroheliogram mode the grating could be set on command to permit the seven individual detectors to observe a variety of wavelengths simultaneously, with a spectral purity of several Ångstroms.

The instrument could achieve spectroheliogram observations with various combinations of field-of-view and time resolutions. These were 5×5 arc min in 5.5 min; 1×5 arc min in 1 min, and 5 arc sec$\times5$ arc min in 5.5 sec; in the stationary mirror mode it could observe a single 5×5 arc sec solar element every 0.041 sec. During each data integration time the continuous mirror scan motion moved the image by 2.5″, half the width of the entrance slit. The description and calibration of the instrument are discussed elsewhere in greater detail (Reeves *et al.*, 1974b; Huber *et al.*, 1974b).

Most theoretical models for the quiet Sun constructed to explain the solar ultraviolet spectrum are based on the assumptions of hydrostatic equilibrium and plane-parallel geometry. These limitations are imposed both by the need for theoretical simplicity, and by the lack of adequate resolution in the instruments, which frequently are not able to resolve the variety of known fine-scale structures. This paper reports some of the more recent EUV observations of quiet regions of the Sun in the ultraviolet and discusses them in terms of the inferred structure.

In large quiet areas of the Sun, which are selected to be devoid of obvious active regions, sunspots, filaments, and coronal holes, the dominant solar structure is the chromospheric network, with inclusions of EUV/X-ray bright points (not currently discernible from ground-based observations) distributed more or less uniformly over the solar disc (Golub *et al.*, 1975). The chromospheric network present in these quiet solar regions has been observed in the EUV from rockets and satellites with various photographic and photoelectric instruments. The observations show that the bright Ca II emission network, observed from the ground to outline large supergranulation cells, has co-spatial bright ultraviolet structures in the characteristic lines and continua of the chromosphere and transition region (Brueckner and Bartoe, 1974; Reeves *et al.*, 1974a). Figure 1 shows a typical set of observations (Reeves *et al.*, 1976) in the polychromatic mode of the Harvard ATM instrument described above. The data were obtained approximately midway to the solar limb on 13 August 1973. The original digital data have been transformed into a 64-level gray scale for pictorial presentation. The chromospheric network can be seen to extend almost unchanged in structure from temperatures characteristic of the Lyman continuum at 10^4 K through C II,

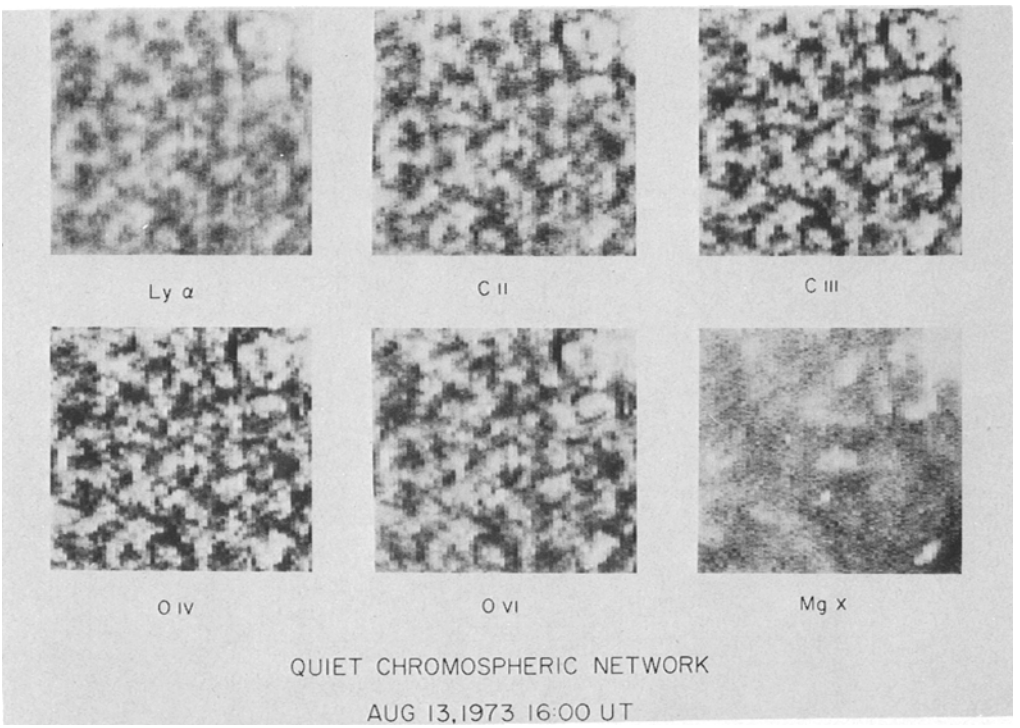

Fig. 1. The chromospheric network observed approximately midway to the limb on August 13, 1973 at 1600 UT.

C III, and O IV to O VI at 3×10^5 K. At temperatures above those characteristic of O VI the appearance of the chromospheric network changes abruptly, and in coronal lines such as Mg X and Si XII it is virtually unrecognizable as a semicontinuous interlocking structure, although occasional remnants of the network can be seen in these and other coronal lines.

The various observations in the EUV are in substantial agreement concerning the general characteristics of the EUV bright network, although there are differences of detail. Rather than primarily addressing the morphological observations of the network, this paper examines the intensities associated with the supergranulation cells. In the remainder of this discussion the boundaries of the supergranulation cells will be referred to simply as network, and the interior regions as cells.

2. Intensity Distribution in Quiet Regions

The distribution of intensities in the 5×5 arc min spectroheliograms of quiet solar regions, such as illustrated in Figure 1, is shown in Figure 2 for O IV at 554 Å. The spatial resolution is 5 arc sec, and the spectral purity at the exit slit is 4.0 Å. Figure 2 shows a frequency distribution which is quite representative of

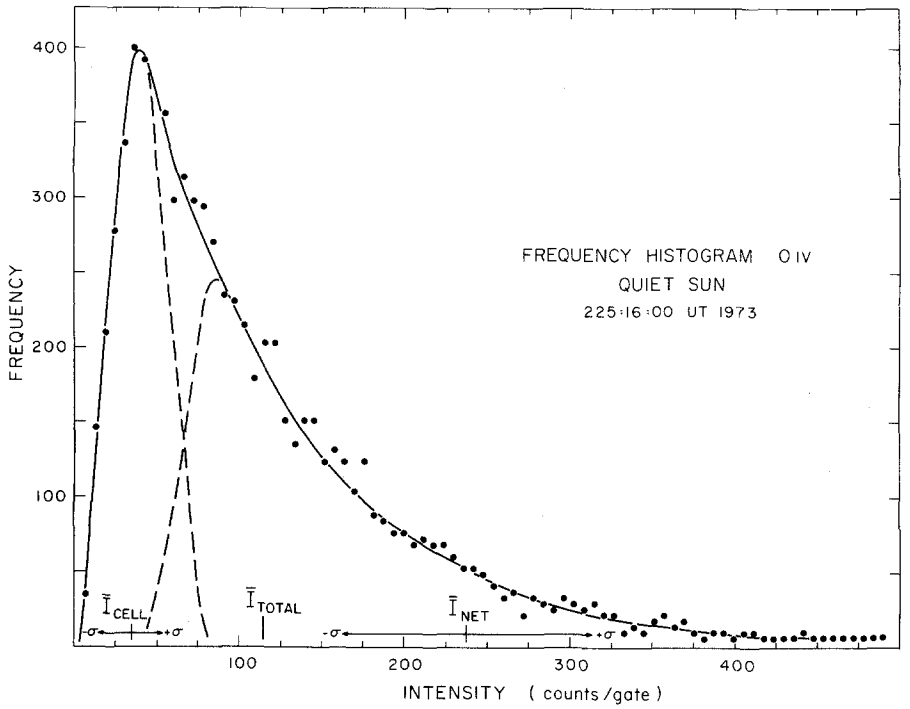

Fig. 2. The distribution of measured intensities in the O IV spectroheliogram of Figure 1.

chromospheric and transition region lines in quiet areas. The range of measured intensities (in counts per 0.041 sec) was linearly divided into approximately 300 intervals and the number of samples in each interval was plotted versus the measured intensity level. The observed frequency distribution has a pronounced maximum, with a tail extending to higher intensities. There is no clear separation into two dominant intensities characteristic of the centers of supergranulation cells and the network to yield a bi-modal distribution, as might perhaps have been expected from the appearance of the spectroheliograms.

Frequency analyses were obtained for many lines in the EUV spectrum for a quiet region on 9 August 1973. These included the lines of the first polychromatic position (C II 1335 Å, Lyα 1216 Å, O VI 1032 Å, C III 977 Å, Ly$_c$ 900 Å, Mg X 625 Å, O IV 554 Å), and also the He I 584 Å, O III 704 Å, N III 991 Å, Ne VIII 780 Å, and the Lyman continuum at 900 Å. Examples of the frequency distributions for some of these wavelengths are shown in Figure 3. The curves have similar shapes for all wavelengths originating from the chromosphere and transition region. We now examine, separately, the details of the intensity distributions arising from network and from cell interiors.

If an intensity level approximately equal to the average intensity in the spectroheliogram is used to construct isophote contours in the original EUV data,

then two separate spatial structures emerge. Large and contiguous areas form the supergranulation cells in which the intensity is systematically less than the average intensity in the entire raster, while the spatial association of intensities greater than the average clearly indicates contiguous structures corresponding to the network. Moreover, the network corresponds very closely to that observed simultaneously from the ground in Ca II (data kindly provided by Haleakala Observatory, Hawaii) and with images from the on-board Hα telescope. The average intensity in the total spectroheliogram is indicated in Figures 2 and 3 as $\bar{I}_{\text{Total}}$.

Calculations of the average intensity for the obvious cell interiors used data from spatial elements one or more resolution elements away from the isophote contour towards the obvious cell interiors. Similarly, the average intensity was calculated for the network regions for intensities greater than that of the isophote

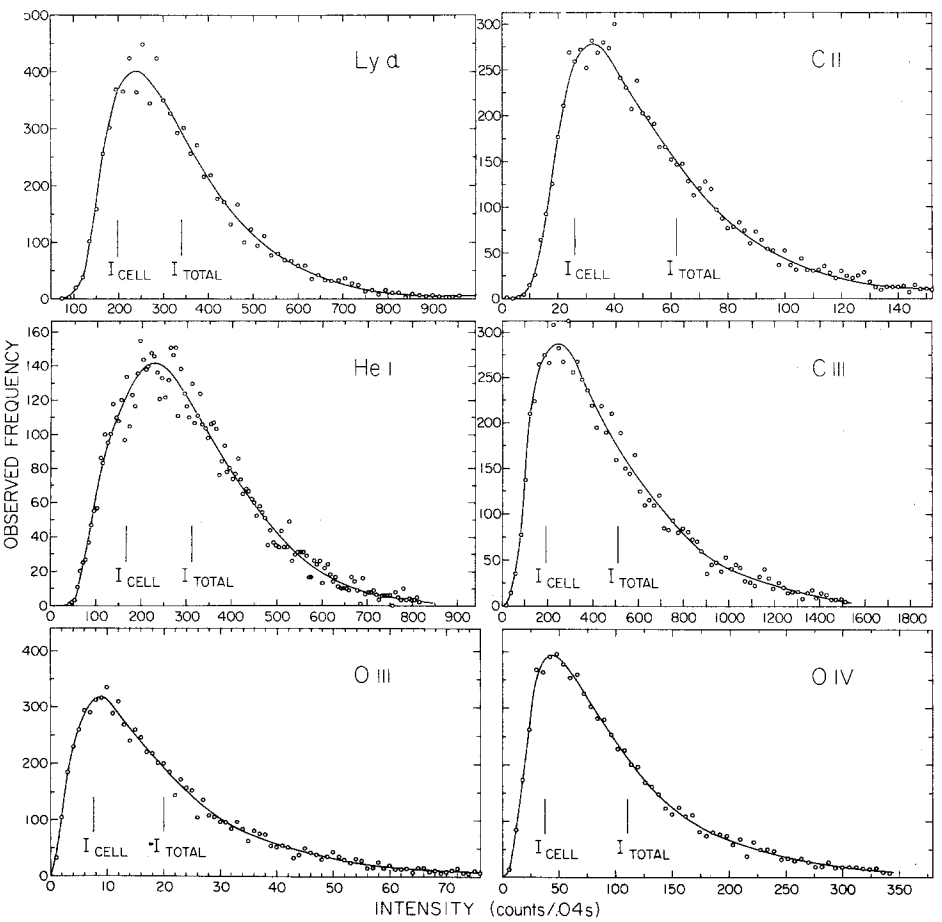

Fig. 3. Intensity distributions for the quiet Sun for representative lines of the chromosphere and transition region on August 9, 1973.

contour. The separate cell and network averages are indicated in Figure 2 for O IV, with the measured standard deviations. For O IV, the average intensity of the cell interior regions corresponds closely to the maximum in the frequency distribution; that is, the most prevalent intensity in a spectroheliogram of the quiet Sun corresponds closely to that arising from the interiors of supergranulation cells.

A similar skewed distribution for spectroheliograms of chromospheric origin has been reported recently (Skumanich *et al.*, 1975) for observations of the statistical distribution of Ca II K core brightness, magnetic field, vertical velocities, and continuum brightness in quiet regions of the Sun. Skumanich *et al.* interpret their distribution for Ca II as a combination of a symmetrical distribution, associated with the supergranulation cell interiors, and a superimposed extended tail, associated with the chromospheric supergranulation cell boundaries (network).

We have used the EUV data from ATM to examine the degree to which the intensity of cell interiors is represented by the most frequency occurring intensity in the distribution, and the normality of the distribution. As described above, isophote contours at the average spectroheliogram intensity were used to select a set of intensities for cell interior regions at least one resolution element from the isophote contour. The average intensity for each set of data ($\bar{I}_{\text{cell}}$) was compared

TABLE I
Characteristics of the intensity distribution from the centers of supergranulation cells

Line	λ cont	Ly α	He I	C II	C III	N III	O IV	O VI
Wavelength	900 Å	1216 Å	584 Å	1335 Å	977	991	554 Å	1032 Å
DOY: 150								
n		819		761	737		810	796
$\bar{I}$		284.22		36.58	285.6		43.19	97.42
σ		70.48		13.18	134.8		24.80	42.21
$\sigma/\sqrt{\bar{I}}$		4.18		3.12	7.97		3.77	4.28
DOY: 221								
n	986	4004	1142	1044	1002	1015	955	1147
$\bar{I}$	23.41	197.0	168.4	27.04	196.2	28.16	36.93	77.61
σ	7.68	49.60	64.71	10.01	90.96	11.51	19.10	35.27
$\sigma/\sqrt{\bar{I}}$	1.63	3.53	4.99	1.92	6.49	2.17	3.14	4.00
DOY: 361								
n		926		939	894		857	1016
$\bar{I}$		68.44		7.58	90.31		21.52	28.91
σ		18.59		3.56	48.17		12.32	13.07
$\sigma/\sqrt{\bar{I}}$		2.24		1.29	5.07		2.66	2.43
Av $(\sigma/\sqrt{\bar{I}})$	1.63	3.32	4.99	1.80	6.51	2.17	3.19	3.57
σ $(\sigma/\sqrt{\bar{I}})$	—	0.99	—	0.46	1.45	—	0.56	1.00

with the most frequently occurring intensity in the spectroheliogram (I_{max}). The average difference between these two measures was less than 15% for chromospheric and transition region lines. He I 584 Å showed the largest difference (about 34%), although the scatter in the helium distribution (Figure 3) makes the evaluation less precise than for other EUV lines. Moreover, helium is somewhat anomalous in the solar spectrum, showing a greater sensitivity to coronal holes than any other lines of the chromosphere or transition region. In Ne VIII the chromospheric network is still clearly observable as a coherent structure at reduced contrast even when allowance is made for the Lyman continuum which underlies the Ne VIII line. Since the temperature associated with Ne VIII (7×10^5 K) is at the top of the range associated with the transition region, and intermediate to quiet coronal values, the intensities derived for the centers of the cells for Ne VIII depart from the most frequent intensity by approximately 50%.

If we examine the intensity distributions in the data from the centers of supergranulation cells, we find that the observed distributions are approximately but not strictly normal. Table I shows the data for three days (identified by Day of Year), distributed throughout the Skylab mission, which were used for the analysis of cell intensity distributions. χ^2 tests for each of the 18 distributions indicated that they were normal within a 0.01 probability. When the distributions were examined for flatness (kurtosis) most wavelengths indicated no significant flatness, with three examples showing a tendency for significant flatness, one for less significant flatness, and one a slight tendency to peak. However, when tested for skewness with the third moment, all of the distributions showed values of $\sqrt{\beta}$ which would indicate that all examples studied should be considered as coming from skewed parent distributions. In all cases the most probable intensity (I_{max}) is to the low-intensity side of the peak of the best-fitting normal distribution curve. In other words, the distribution of intensities selected from the centers of supergranulation cells is approximately normal, but shows a definite tendency to an asymmetrical distribution like that from the entire spectroheliogram. The skewness is further confirmation of the average 15% separation of $\bar{I}_{cell}$ and I_{max} described above. The observed distributions resemble a Poisson shape; however the data would be expected to follow a normal distribution quite closely.

The ratio of the calculated standard deviation from each data sample to that expected on the basis of sampling statistics ($\sqrt{\bar{I}}$) is always greater than 1, and in one sample reaches a value of nearly 8 (see Table I). The average value ($\sigma/\sqrt{\bar{I}}$) for all of the lines is approximately 3.6. This excess 'noise' in the intensity data is attributed to finer scale structure than can be resolved with the 5 arc sec resolution of the HCO instrument, but which is known to exist from high-resolution magnetograms and Hα images. However, to a reasonable approximation the intensities from the centers of supergranulation cells can be assumed to arise from a rather homogeneous structure (on the scale of 5 arc sec), and a future paper will deal with the modelling of these regions on the basis of a plane-parallel atmosphere.

3. Observations of the Bright EUV Network

The analysis of the intensities of EUV lines of the chromosphere and corona from the centers of supergranulation cells indicates that these regions may be considered to have a uniform and characteristic structure, to a reasonable approximation. The chromospheric network was also examined in the same EUV lines to investigate the degree to which the network boundary regions can also be ascribed a single characteristic intensity, and hence structure.

The general similarity between the appearance of the bright EUV network and the Ca II K network has been supported by several sets of observations (Reeves *et al.*, 1974a; Brueckner and Bartoe, 1974). That is, for spectroheliograms obtained at nearly the same time there is a great similarity between the general network *pattern* seen in the EUV and the bright emission of Ca II. It is clear, however, that there are always differences in the exact details, which are assumed to arise from the lack of complete simultaneity. Recent rocket observations at high spatial resolution have proposed that the EUV network is significantly more diffuse than observed in Ca II (Brueckner and Bartoe, 1974). This spreading of the network with temperature (or height) will be examined in detail later in this paper.

Since the ATM complement of experiments included in Hα telescope it was possible to compare the bright EUV network with Hα images obtained almost simultaneously. The dark mottles seen in Hα photographs have been associated with spicules or spicule clumps occurring in the calcium network (Beckers, 1968). Spicules are seen most clearly in offband Hα, especially the blue wing, and are not particularly visible near the center of the Hα profile. The 5 arc sec resolution of the current EUV instrument does not resolve the EUV contribution from individual spicules, nor does the Hα telescope provide superior data on individual mottles or fibrilles. The present data simply confirm that the EUV chromospheric network corresponds to the supergranulation boundaries seen in Ca II, as outlined by the dark mottles in Hα, and the correlation is best where the data are nearest in time. However, the brightest network elements seen in O IV do not necessarily coincide with the darkest mottles in Hα, and hence Hα (as observed with the ATM 0.7 Å Fabry–Perot filter) does not provide a suitable guide to the brightest spicules or spicule clumps in the EUV.

The fine details in the structure of the EUV network can be seen to evolve on time scales of 5 min, the basic raster repetition rate. If the EUV network is considered to be composed of spicules and interspicular material, then this evolution on a time scale of a few minutes is consistent with the known evolution time for spicules. Without much higher spatial resolution it is not possible to distinguish between spicules and interspicular material when the network is viewed normally near the center of the disc. Investigations are in progress (Mariska and Withbroe, personal communication) to obtain some distinction through the general course of center-to-limb intensity changes in transition region lines.

If the intensities along a section of network are examined, large changes are observed for image elements separated by only a few arc seconds. For a full 5 arc min spectroheliogram in quiet regions of the Sun, the O IV intensities can span a dynamic range of several hundred, and in the case of small inclusions of Hα bright regions the range can exceed 1500:1. (The very intense bright knots in active regions can increase the ratio still another order of magnitude, and flare observations yet further.)

Figure 4 shows the intensities along two representative network elements. Intensities were recorded strictly simultaneously for each image element at all wavelengths, although the scanning nature of the raster pattern convolves a small time evolution with spatial changes. There are significant changes in the relative

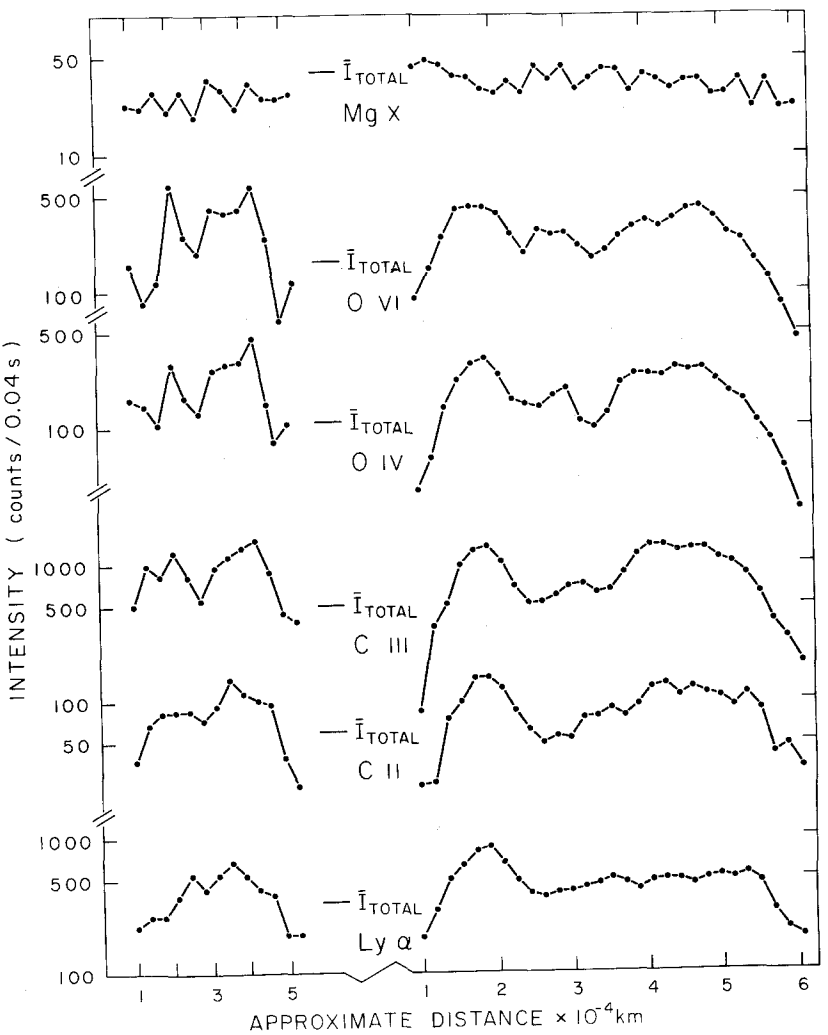

Fig. 4. EUV intensity changes along the length of two examples of chromospheric network. Distances are approximate.

intensities along the length of the network feature in all of the EUV lines, although the individual enhancements show many changes of intensity which are not monotonic with increasing temperature of formation of the EUV line. Isophote contours or pictorial representations frequently show a 'gap' in the network for one line, while another line may show the network element to be 'continuous'. The apparent continuity of the network is strongly dependent on the contrast between the network and cell elements and the intensity levels chosen to construct the spectroheliograms. The apparent discontinuity of the network when observed photographically (Brueckner and Bartoe, 1974) can be the result of the more limited dynamic range and level of exposure characteristic of Schumann-type films. In any event, the network is highly structured with very significant changes in intensity from point to point.

If the EUV network is the reflection of predominant emission from transition sheaths around individual spicules, then the known spatial inhomogeneities in the spicule distribution would account qualitatively for the variations of the observed EUV intensities along the length of network elements.

4. Width of the Chromospheric Network

Although the network exhibits considerable variations in the detail of its structure, an attempt was made to determine an average width for the network in the EUV region as a function of the formation temperature of the line. A large number of network elements were examined both in the direction of the mirror scan (yielding 2.5 arc sec measurement separations) and transverse to that direction (with 5 arc sec line separations). For each of the 116 network elements studied the full width of half peak intensity was determined from a fit to the

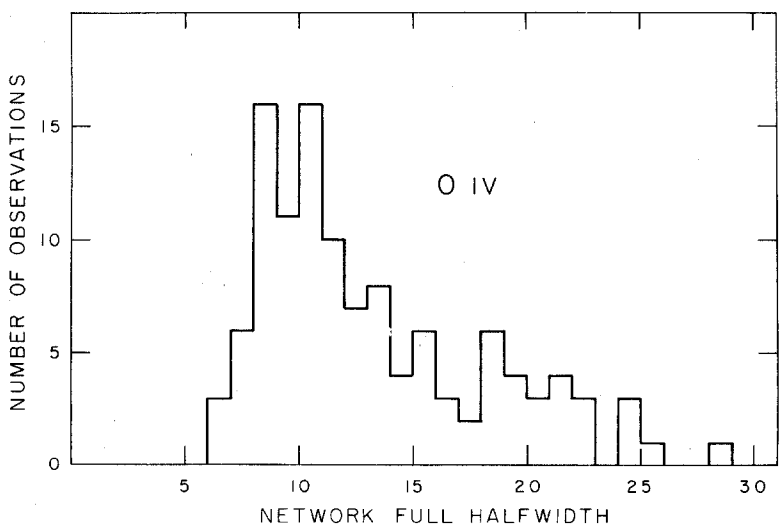

Fig. 5. Observations of the full half width (FWHM) of the chromospheric network observed in O IV at 554 Å.

intensity profile across the network element for O IV. The results are shown in the histogram of Figure 5, which indicates an average measured halfwidth of 10 arc sec, with a tail extending to 30 arc sec. Since the instrumental profile has a full-width half maximum of 5 arc sec for a point source, all structures will appear to have this limiting lower range, although halfwidths for structures greater than 5 arc sec will be correctly determined.

Examples of well-defined, isolated, and 'typical' contrast network regions were selected for quantitative evaluation from the data for several days distributed throughout the ATM mission. Network samples were traversed nearly in the direction of the mirror line scan motion, since in that axis data readouts from the 5 arc sec slit were obtained every 2.5 arc sec of displacement. The intensity profile across the network was plotted and the width of the network was examined at the 1/2, 1/*e*, and 1/4 intensity intervals between the peak intensity and the neighboring cells. In each case the width was measured relative to that obtained for O IV at the same relative intensity (1/2, 1/*e*, or 1/4 width) to avoid the scatter in widths from one network structure to another. No appreciable differences were observed among the relative widths at 1/2, 1/*e*, and 1/4 intensities. The average value of the width for the network elements is plotted in Figure 6 with the associated standard deviations.

The numerical data show that the width of the network elements observed in He I, and the lines and continuum of the Lyman series of hydrogen, are not appreciably broader on the average, than when viewed in the upper chromospheric and transition region lines. In Lyman α, the average width of the network, which we infer from our data to be approximately 10 arc sec, is less than the value of 20 arc sec reported by Prinz (1974) from a photographic rocket experiment. Furthermore, there is some indication that our observations indicate a slightly

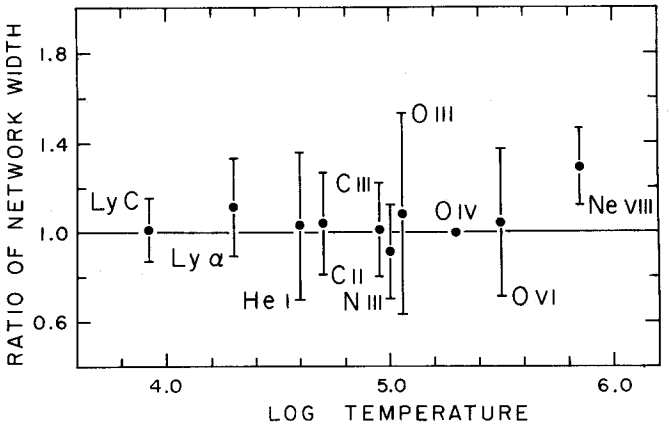

WIDTH OF THE CHROMOSPHERIC NETWORK RELATIVE TO O IV

Fig. 6. The range of chromospheric network widths relative to the width in O IV for selected network samples.

greater width for the chromospheric network when observed in higher temperature lines such as Ne VIII. Since the contrast in the network decreases rapidly for lines formed at temperatures greater than 3×10^5 K and approaching the overlying coronal temperatures, the properties of Ne VIII emission from the network are difficult to determine. Ne VIII emission is formed in the upper limits of the zone referred to as the transition region, and the network is not discernible in any systematic way in lines of higher temperature formed in the corona.

In an earlier paper (Reeves *et al.*, 1974a) we interpreted the spatial preservation of the chromospheric network through the lines of the transition region, and the essential absence of network structure at coronal temperatures, as evidence of the vertical magnetic field in the network and a rapid spreading to a horizontal configuration in the corona, as discussed by Kopp and Kuperus (1968), and others. There is no experimental evidence of the implied spreading of the field at temperatures below 7×10^5 K as would perhaps be implied by that model.

More recently Gabriel (1976) has suggested a theoretical model in which the primary transition region forms a closed 'mushroom-shaped' cap over the boundaries of the supergranulation cells. The model predicts a constant width to the network of approximately 10 arc sec for lines formed at temperatures up to 6.3×10^5 K, comparable to Ne VIII. The model further suggests that the network boundary should be brightest on the outer edges for optically thin lines, with a width of about 1 arc sec. The resolution of our ATM instrument would not be adequate to discern such fine-scale detail, but, as Gabriel points out, that detail is based on a purely idealized case.

While the model proposed by Gabriel is supported in many details by our observations, no theory yet accounts for the spicules observed along the network boundaries as dark mottles in Hα, and presumed to be the source of the large changes in EUV intensities from point to point along the network observed by both the HCO and NRL experiments on ATM.

Since the width of the network elements does not appear to be dependent on temperature of formation of the line in which it is observed, and since the general pattern of the network is also quite similar in these same lines, it follows that the area of quiet solar regions occupied by the network is the same for the EUV lines of the chromosphere and transition region. From the results of Skumanich *et al.* (1975) the network observed in the bright core of Ca II K occupies about 40% of the area of the average quiet Sun. Our estimates from O IV (see Section 6) indicate that the EUV network occupies about 46% of the quiet Sun disc. The Ca II observations were made with a spatial resolution of 2–5 arc sec and the EUV observations at 5 arc sec.

5. Contrast between the Network and Cells

The question of the contrast between elements of the chromospheric network and the centers of cells can be examined from data obtained when the astronauts were

able to obtain wavelength scans from individual network and cell elements. Two such occasions have been examined. The first occurred intentionally when Astronaut Owen Garriott used the Hα telescope to locate a well-defined network element in Hα on 13 August, and obtained sequential spectral scans as the slit of the Harvard instrument was stepped across the Hα network in 5 arc sec steps. The second occasion occurred during random wavelength scans in a quiet region near the disc center in association with a calibration rocket flight. In both instances the network element scanned was of intermediate intensity in the EUV, and was well-defined and isolated with cell structure on either side.

Figure 7 shows the ratio of the intensity in the network to the intensity in a nearby cell element, where the cell intensity corresponded approximately to the average cell intensity. The 'contrast' is therefore not nearly as great as can be found between selected network and cell elements. The measured intensity ratios are plotted against the effective temperature, that is, the temperature at which the ion achieves its maximum abundance in the calculations of ionization equilibrium. As nearly as practicable, the data represent the average network (with all the limitations on homogeneity of network expressed throughout this paper). Considerable scatter is observed in the data, even though two successive wavelength scans of the network are averaged together. The contrast ratio is based on the measured count level for the wavelength scans, and in all cases the intensity for each line is that after any underlying continuum has been removed by computer

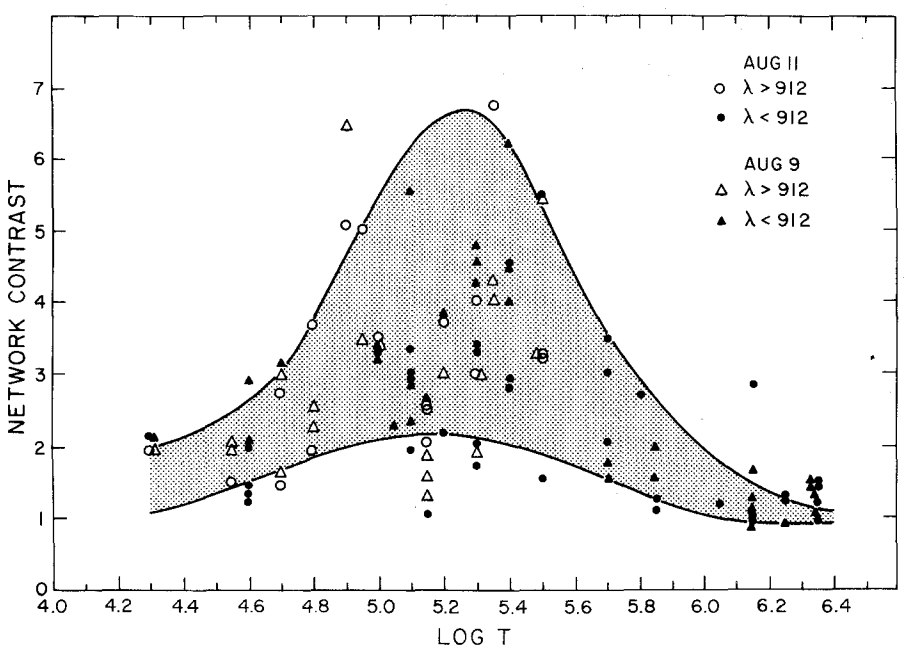

Fig. 7. Contrast between the intensities of representative network and supergranulation cell interiors. Solid points are for wavelength below the Lyman limit and open circles for wavelengths longwards of the Lyman limit.

processing. There does not seem to be any systematic difference in the contrast for lines above and below the Lyman limit, implying no significant absorption from the Lyman continuum in the network elements.

The contrast data from the wavelength scans support the qualitative aspects of the spectroheliograms, namely, that the network achieves its maximum contrast in lines arising from the transition region about 2×10^5 K, and that it is well-defined in lines of the chromosphere and transition region extending up to temperatures of 7×10^5 K corresponding to Ne VIII. In lines such as Ne VII and Ne VIII the chromospheric network pattern is still recognizable, albeit at reduced contrast, since these ions exhibit intermediate morphology between transition region structures and the diffuse structures seen in coronal lines such as Mg X and Si XII (where the network pattern is definitely unrecognizable).

Figure 8 shows a plot of the contrast in the network elements of Figure 7 for the observed lines and continuum of the Lyman series of hydrogen ($1s\ ^2S_1 - np\ ^2P^0_{1/2}$). The lines of the Lyman series have had any underlying continuum removed, and the error bars represent estimates of uncertainty based on counting statistics. The data show some small tendency for the contrast between the network and the cells to be higher in the continuum than in the lower (and better resolved) members of the Lyman series, although there does not seem to be any significant change in contrast for different wavelengths in the Lyman continuum. In other words, the relative shape of the Lyman continuum, and hence the effective colour temperature, are apparently the same for line-of-sight observations into the cells or network.

Noyes and Kalkoffen (1970) have shown that the slope and intensity of the Lyman continuum can be used to derive an estimate of the color temperature in

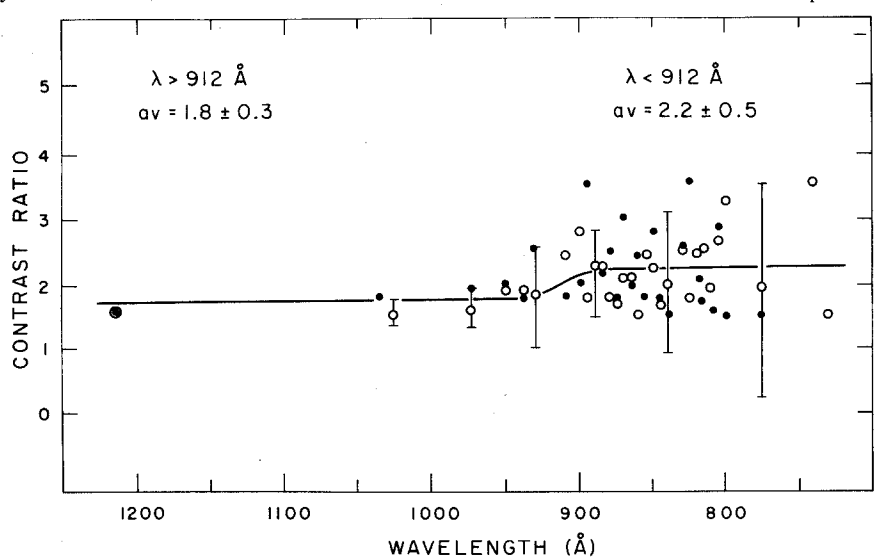

Fig. 8. Contrast between the network of and cell interiors for the lines and continuum of the Lyman series. Solid circles represent data for August 13 and open circles for August 11, 1973.

the region of formation, and also an estimate of the departure coefficient (b_1). The departure coefficient for the quiet Sun spectrum, averaged over chromospheric structure, was determined to be $b_1 \approx 270$ from the data from OSO IV at a spectral resolution of 1 arc min (Vernazza and Noyes, 1972). The current ATM data are not sufficiently precise to permit an evaluation of any change in the effective departure coefficient associated with the two-fold increase of intensity in the network sample. A temperature of 8200 K was determined from the slope of the Lyman continuum, which agrees with the value of 8300 K of Noyes and Kalkoffen (1970) within our uncertainty. A temperature change of approximately 295 K will account for the differences in the absolute intensity between the cell interiors and the network at the head of the Lyman continuum; however, the commensurate change in the slope of the Lyman continuum is only 9.8%. The ATM data therefore do not permit an estimate of any change in the departure coefficient or effective density between the cell interiors and the network in the region of formation of the Lyman continuum near 10^4 K.

The electron density at higher temperatures can be inferred from line ratios in beryllium-like species such as C III and O V, where the lines originate from levels whose populations are sensitive to electron density, as discussed by Munro (1973). Interpretation of the measured intensity ratios in terms of electron density is also very sensitive the the atomic parameters (Loulergue and Nussbaumer, 1974, 1976; Jordan, 1974). Electron densities were determined for C III (λ 1176/λ 977) and O V (λ 760/λ 630), using the data of Munro (1973), from sets of spectral scans in cell interiors and network boundaries for two quiet solar regions. The average values of the measured electron density for the cell interiors and network for these two temperature regions are shown in Table II. The uncertainty listed is the standard deviation for the two measurements. A more complete analysis of the electron density measurements using the C III diagnostics and the ATM data is in progress (Dupree *et al.*, 1976).

Within the uncertainties of the determinations the measured values for the electron density for C III ($\log T_e = 4.8$) and O V ($\log T_e = 5.4$) are the same for both the cell interiors and the network. Although not statistically significant, the measured electron density has a tendency to be higher in the cell interiors than it

TABLE II

Averaged electron density and temperatures for two sets of observations in the quiet Sun

	Network	Cell
Electron density		
C III ratio	$(1.45 \pm 0.21) \times 10^{10}$	$(1.50 \pm 0.71) \times 10^{10}$
O V ratio	$(0.75 \pm 0.35) \times 10^{10}$	$(2.32 \pm 2.3) \times 10^{10}$
Electron temperature		
Si XII/Mg X	1.7×10^6 K	1.7×10^6 K

is in the network, as is observed also in the more extensive analysis of Dupree *et al.* (1976).

The electron temperature in the solar plasma can also be inferred from the intensity calculated on the basis of fractional concentration of the ion as a function of temperature, assuming ionization equilibrium. Theoretical calculations (Withbroe, 1971) show that the ratio of the lithium-like species Si XII (499 Å) to Mg X (625 Å) is sensitive to temperature up to 2.5×10^6 K. Calculations of this ratio were carried out for the network and cell interiors in the same regions as for C III and O V. The average values for the cell interiors and network are shown in Table II. The coronal temperature derived from line ratios is subject to uncertainties in both the instrumental calibration and the theoretical ratios predicted from calculations involving ionization equilibrium. The temperature of the quiet corona derived from these data samples is higher than the value of 1.1×10^6 K derived from center-to-limb studies in quiet regions (Mariska and Withbroe, 1975). Regardless of the actual value for the estimated temperature it does appear that the quiet coronal temperature over cells and network is not appreciably different.

6. The Relative Intensity Contribution of the Network

The EUV data were examined to estimate the relative contribution of the network and cell interiors to the average intensity from the quiet Sun near disc center. Since O IV is in the region of maximum contrast between the network and cell interiors, it was used to define the location of the network. A threshold

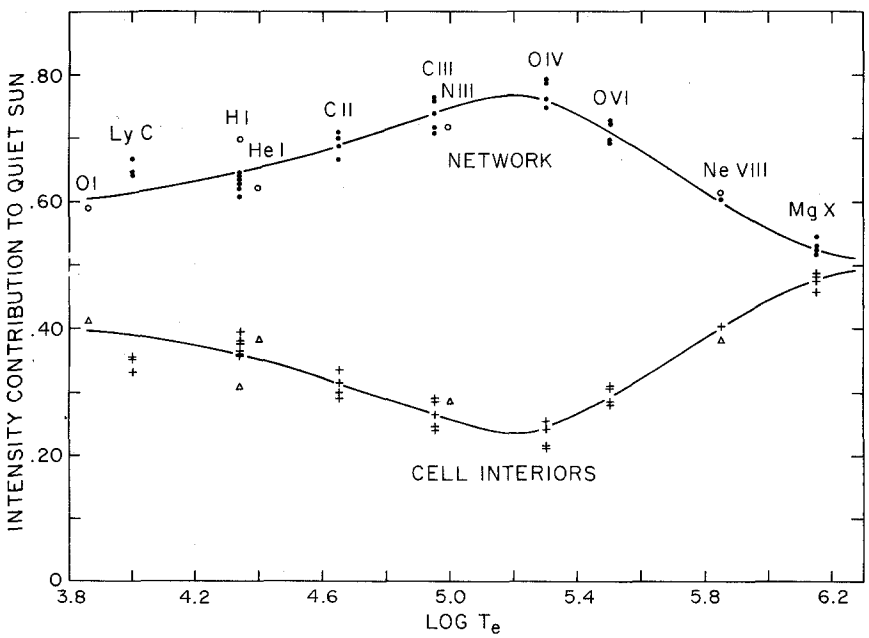

Fig. 9. The contribution of the network and cell interior regions to the intensity of the average quiet Sun.

intensity near the average intensity in the spectroheliogram and close to the upper range of intensity associated with cell interiors (see, for example, an intensity of 85 in the dashed curve of Figure 2) was used to define the network in a series of spectroheliograms. For each wavelength examined, the intensity of O IV from the same picture element was used to sort the intensity for that species into the two categories, cell interiors and network. As the threshold intensity is varied between the two limits discussed above ($85 \leq I \leq \bar{I}$ in Figure 2) the number of points in the network, and hence the area associated with the network varied from 38% to 50%. For the intensity contributions discussed here the area of the network was approximately 46%.

The percentage contributions from the network and cell interiors are shown in Figure 9 for the five sets of data obtained throughout the mission.

The network contributes about 60% of the intensity of the quiet Sun at the low temperature extremes of 10^4 K, but for lines near the maximum of the contrast between network and cell interiors, the network contributes approximately 75% of the average quiet Sun values. For lines arising from the corona the contribution from the network is very nearly 50%, that is, there is no consistent intensity contribution from the corona overlying the chromospheric network. The contribution values illustrated in Figure 9 are not strongly dependent on the exact value of the threshold intensity chosen for O IV. There is some scatter in the data, arising from statistical fluctuations, as well as from uncertainties in the temperature of formation assigned to different lines.

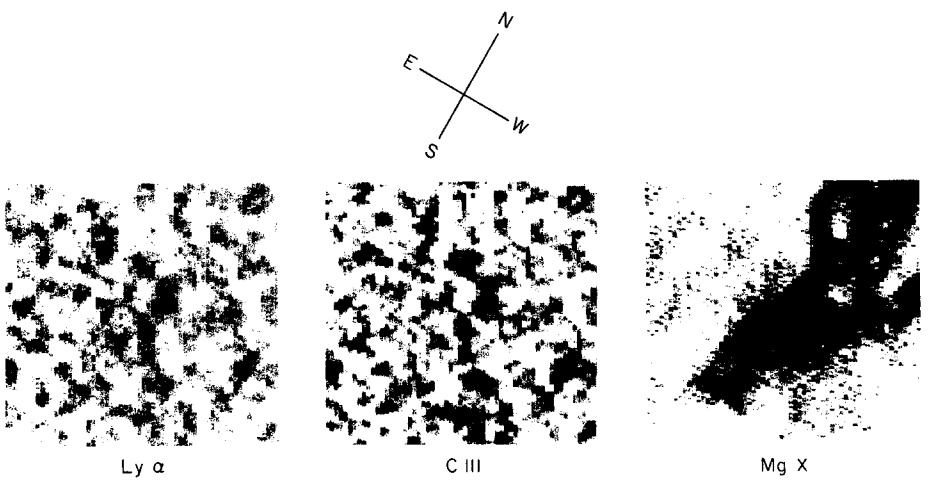

Fig. 10. The chromospheric network in the region of a coronal hole.

7. Cells and Network in Coronal Holes

Coronal holes appear as larger regions of reduced coronal intensity, particularly visible in EUV lines such as Mg X and Si XII, and in the X-ray heliograms obtained from rockets and more recently from ATM. Figure 10 shows several of the spectroheliograms obtained on 22 November near disc center. The Mg X

TABLE III
Intensities of cells in coronal holes

Line	Wavelength (Å)	Coronal hole intensity (cts/0.040s)	Quiet region intensity (cts/0.040s)
C II	1335	12.11±4.58	11.35±4.31
L α	1216	89.74±20.35	87.22±22.60
C III	977	123.45±52.46	116.23±54.93
O IV	554	25.45±12.56	25.05±12.55
O VI	1032	36.54±14.33	35.49±14.34

image shows the presence of a large coronal hole, and the C III and Ly α images show the underlying chromospheric network structure. The hole is located at disc center and extends well beyond the field of view of this instrument, being well defined in simultaneous X-ray images obtained by the American Science and Engineering department.

As reported previously (Huber *et al.*, 1974a), the chromospheric network and its upward extension into the transition region remain very well defined in coronal holes. Table III shows the measured mean intensity for the interior of chromospheric cells examined for the two distinct regions inside and outside of the coronal hole, together with the calculated standard deviation for each set of data.

The analysis shows remarkable consistency for the intensities of the cell interiors, whether located within coronal holes or in quiet regions. For the above lines, we can conclude that the observed differences in intensity distributions observed in coronal holes (Huber *et al.*, 1974a) are probably due to changes in the network. It now appears that the large differences in chromospheric and transition region line intensities for the network elements in regions of coronal holes may not be observed in all cases. However, we do consistently observe an increase in the network intensity of approximately a factor of 2 for intensities several times the average intensity of cell interiors for coronal hole regions relative to quiet regions for observations in Lyman α and the Lyman continuum. Further investigations of a variety of coronal holes observed throughout the Skylab mission are in progress and will be reported separately.

8. Conclusions

The current investigations of the quiet Sun suggest that the interiors of supergranulation cells have an intensity which is quite constant, even including regions

of coronal holes. The intensity distribution from cell interiors is approximated by a normal distribution, but with a standard deviation larger than that to be expected on the basis of random sampling. The chromospheric network, on the other hand, shows much larger spatial variations in intensity from point to point, and has a decidedly skewed intensity distribution. The network is characterized by a large intensity contrast relative to the cell interiors as a function of temperature of formation, which maximizes near temperatures of 2×10^5 K. However, the network structure can be discerned in lines up to Ne VIII at approximately 7×10^5 K, although at greatly reduced contrast. The width of the network elements is independent of temperature over the range 10^4 to 3×10^5 K and probably approaching 7×10^5 K, the limit to which network structure can be traced consistently. The contribution of the network to the intensity of the quiet Sun is a marked function of temperature of formation, increasing from approximately 60% at 10^4 K to 75% at 2×10^5 K, and then dropping to 50% for lines of coronal origin. Measurements of electron density and overlying coronal temperatures indicate similar values for cell interiors and network viewed normal to the solar surface. The results are consistent with the network model proposed by Gabriel (1976).

Acknowledgements

The author wishes to acknowledge the help of Mrs Pamela Wetherbee in the numerical analysis of the data, and thanks Drs R. W. Noyes and G. L. Withbroe for several discussions of the manuscript. Continuing thanks are due to the engineers and scientists of the HCO ATM group for their years of effort in building and operating the instrument, and to the personnel of the Marshall Space Flight Center and the Johnson Spacecraft Center, especially in data acquisition and processing. This work was supported by the National Aeronautics and Space Administration under contract NAS 5-3949.

References

Beckers, J. M.: 1968, *Solar Phys.* **3,** 367.
Brueckner, G. E. and Bartoe, J-D. F.: 1974, *Solar Phys.* **38,** 133.
Dupree, A. K., Foukal, P. V., and Jordan, C.: 1976, *Astrophys. J.* (in press).
Gabriel, A. H.: 1976, *Phil. Trans. Roy. Soc. A* (in press).
Golub, L., Krieger, A. S., and Vaiana, G. S.: 1975, *Solar Phys.* **42,** 131.
Huber, M. C. E., Foukal, P. V., Noyes, R. W., Reeves, E. M., Schmahl, E. J., Timothy, J. G., Vernazza, J. E. and Withbroe, G. L.: 1974a, *Astrophys. J.* **194,** L115.
Huber, M. C. E., Reeves, E. M., and Timothy, J. G.: 1974b, *Space Optics* (Proc. 9th Int. Cong. of the Int. Comm. of Opt.); Nat. Acad. Sci., 33.
Jordan, C.: 1974, *Astron. Astrophys.* **34,** 69.
Kopp, R. A. and Kuperus, M.: 1968, *Solar Phys.* **4,** 212.
Loulerge, M. and Nussbaumer, H.: 1974, *Astron. Astrophys.* **34,** 225.
Loulerge, M. and Nussbaumer, H.: 1976, *Astron. Astrophys.* (in press).
Mariska, J. T. and Withbroe, G. L.: 1975, *Solar Phys.* **44,** 55.
Munro, R. H.: 1973, Ph.D. Thesis, Harvard University.
Noyes, R. W. and Kalkoffen, W.: 1970, *Solar Phys.* **15,** 120.

Prinz, D. K.: 1974, *Astrophys. J.* **187,** 369.
Reeves, E. M., Noyes, R. W. and Withbroe, G. L.: 1972, *Solar Phys.* **27,** 251.
Reeves, E. M., Foukal, P. V., Huber, M. C. E., Noyes, R. W., Schmahl, E. J., Timothy, J. G., Vernazza, J. E. and Withbroe, G. L.: 1974a, *Astrophys. J.* **188,** L27.
Reeves, E. M., Timothy, J. G. and Huber, M. C. E.: 1974b, *Proc. S.P.I.E.* **44,** 159.
Reeves, E. M., Vernazza, J. E., and Withbroe, G. L.: 1976, *Phil Trans. Roy. Soc. A* (in press).
Skumanich, A., Smythe, C., and Frazier, E. H.: 1975, *Astrophys. J.* **200,** 747.
Vernazza, J. E. and Noyes, R. W.: 1972, *Solar Phys.* **22,** 358.
Withbroe, G. L.: 1971, *Solar Phys.* **18,** 458.